

doi: 10.12029/gc20190609

余宇伟, 朱祥坤, 何源, 万洪清. 2019. 日喀则蛇绿岩中辉长-辉绿岩成因及慢速扩张脊环境[J]. 中国地质, 46(6):1372-1383.

She Yuwei, Zhu Xiangkun, He Yuan, Wan Hongqing. 2019. The formation of gabbro and diabase in the Xigaze ophiolite: Implications for a slow-spreading ridge[J]. *Geology in China*, 46(6):1372-1383 (in Chinese with English abstract).

日喀则蛇绿岩中辉长-辉绿岩成因及慢速扩张脊环境

余宇伟¹, 朱祥坤¹, 何源^{1,2}, 万洪清^{1,2}

(1. 中国地质科学院地质研究所, 北京 100037; 2. 中国地质大学地球科学与资源学院, 北京 100083)

摘要: 日喀则蛇绿岩位于雅鲁藏布构造带中段, 其成因和构造环境仍存在较大争议。日喀则蛇绿岩下部为蛇纹石化地幔橄榄岩, 壳幔过渡带缺失超镁铁质堆晶岩。少量辉长岩脉呈块状或韵律结构并侵入到地幔橄榄岩和辉绿岩中。辉绿岩呈席状岩床侵入到地幔橄榄岩之上, 且少量辉绿岩脉侵入到下覆的地幔橄榄岩中。通过野外关系和地球化学研究, 日喀则辉长岩可能并不是洋壳中岩浆房原位结晶堆积而成, 而是深部位置岩浆囊经过不同程度分异演化形成富晶岩浆并向上侵入的结果。而席状辉绿岩床则是基性岩浆沿着构造薄弱面顺层侵入的结果。拆断层可能导致了岩石圈地幔抬升和剥露, 进而引起下覆软流圈地幔减压熔融和岩浆上侵。日喀则辉长-辉绿岩形成于慢速扩张脊较小规模的岩浆供应和不连续的岩浆侵入。

关键词: 辉绿岩; 辉长岩; 蛇绿岩; 日喀则; 雅鲁藏布; 洋中脊; 慢速扩张; 地质调查工程; 青藏高原

中图分类号: P584; P595 **文献标志码:** A **文章编号:** 1000-3657(2019)06-1372-12

The formation of gabbro and diabase in the Xigaze ophiolite: Implications for a slow-spreading ridge

SHE Yuwei¹, ZHU Xiangkun¹, HE Yuan^{1,2}, WAN Hongqing^{1,2}

(1. *Institute of Geology, Chinese Academy of Geological Sciences, Beijing 100037, China*; 2. *School of Earth Science and Resources, China University of Geosciences, Beijing 100083, China*)

Abstract: The Xigaze ophiolite is located in the central segment of the Yarlung Zangbo Suture Zone, and its genesis and tectonic setting remain controversial. The ophiolite has a serpentinized peridotites in the lower part, and the ultramafic cumulates are absent in the mantle-crust transition zone. Small amounts of gabbro dikes with isotropic or rhythmic textures intruded into the mantle peridotites or diabase sills. The diabase sills generally intruded along the interface of the mantle peridotites or intruded into the mantle peridotites as diabase dikes. Based on studies of field relationships and geochemical features, the authors hold that, the Xigaze gabbro dikes, instead of being formed by in-situ crystallization of magma chamber in the oceanic crust, might have resulted from the intrusion of crystals-enriched magmas from magma pockets which were distributed in crust-mantle boundary and evolved in variable degrees into silicate-rich minerals. The diabase sills might have been formed from the intrusion of mafic magmas along the structurally weak boundary. The detachment faults probably resulted in the uplift and exhumation of the upper mantle which

收稿日期: 2018-07-29; 改回日期: 2019-04-21

基金项目: 中国地质调查局项目(121201102000150069)和国家自然科学基金(41603022)共同资助。

作者简介: 余宇伟, 男, 1983年生, 博士生, 助理研究员, 研究方向为蛇绿岩与豆荚状铬铁矿成因研究; E-mail: sheyuwei@cags.ac.cn。

triggered the upwelling and partial melting of asthenospheric mantle. The gabbro dikes and diabase sills in the Xigaze ophiolite might have originated from small amounts of supply and discrete intrusion of magmas in a slow-spreading ridge.

Key words: diabase; gabbro; ophiolite; Xigaze; Yarlung Zangbo; MOR; slow-spreading; geological survey engineering; Qianghai-Tibet plateau

About the first author: SHE Yuwei, male, born in 1983, doctor, assistant researcher, engages in the study of ophiolite and podiform chromitite; E-mail: sheyuwei@cags.ac.cn.

Fund support: Supported by China Geological Survey Program (No. 121201102000150069) and Natural Science Fund of China (No. 41603022).

1 引言

蛇绿岩是一套可以和现代大洋岩石学圈对比的特殊岩石组合,代表了上地幔和古洋壳的残余(Coleman, 1977)。1972举办的Penrose会议定义蛇绿岩剖面从下到上为:地幔橄榄岩、超镁铁质杂岩、层状-块状堆晶辉长岩、席状辉绿岩墙群、枕状玄武岩、硅质深海沉积岩。然而,这套定义的标准蛇绿岩剖面与世界上大多数地区出露的蛇绿岩特征并不一致(Nicolas et al., 1981)。早期阶段,有学者认为蛇绿岩形成于大洋中脊扩张中心(Mid-ocean ridge 环境)(Coleman, 1971; Dewey and Bird, 1971)。随着地球化学测试手段的发展,研究发现很多蛇绿岩中镁铁质岩石具有与岛弧玄武岩相同的地球化学特征,从而认为其形成于俯冲带环境(Suprasubduction Zone 环境)(Miyashiro, 1973; Pearce et al., 1975; Alabaster et al., 1982)。蛇绿岩一般沿着碰撞缝合带和造山带出露,是板块拼合的标志性岩石。Dilek and Furnes(2011)根据蛇绿岩的地质特征与地球化学特征划分蛇绿岩的成因类型,包括:(1)非俯冲型蛇绿岩(Subduction-unrelated ophiolite),这种类型的蛇绿岩又细分为大陆边缘型(Continental Margin-type),洋中脊型(MOR-type)和地幔柱型(Plume-type);(2)俯冲型蛇绿岩(Subduction-related Ophiolite),这种类型包括俯冲带型(Suprasubduction Zone-type)和火山弧型(Volcanic-arc-type)。这些分类说明蛇绿岩的成因比较复杂,受到构造环境以及就位机制等多重因素的影响。

雅鲁藏布碰撞缝合带自东向西出露一系列蛇绿岩体,而该蛇绿岩带中段的日喀则蛇绿岩保存较高比例的洋壳部分(Nicolas et al., 1981; 王希斌等,

1987)。根据野外地质和地球化学研究,日喀则蛇绿岩被认为形成于洋中脊环境(Girardeau et al., 1985; 陈根文等, 2003; 牛晓露等, 2006; Zhang et al., 2016; Liu et al., 2016)。然而,日喀则蛇绿岩镁铁质岩石的地球化学特征也存在与俯冲作用有关的岛弧型特征,因此很多学者认为日喀则蛇绿岩形成于俯冲带环境(Aitchison et al., 2000; Dubois-Cote et al., 2005; Guilmette et al., 2009; Bedard et al., 2009; Hebert et al., 2012; 李文霞等, 2012; Dai et al., 2012, 2013)。日喀则蛇绿岩中辉长岩和辉绿岩的野外地质和地球化学特征与经典的阿曼蛇绿岩明显不同(Nicolas et al., 1981, 1994),本文将提供新的野外地质证据和地球化学数据来解释日喀则蛇绿岩中辉长-辉绿岩的成因以及对构造环境的启示。

2 地质背景

青藏高原由一系列地体构成,从南向北包括拉萨地体、羌塘地体、松潘-甘孜地体、昆仑-祁连山地体(图1a)(潘桂堂等, 2002)。雅鲁藏布构造带位于青藏高原最南端,介于拉萨地体和印度大陆之间,以一条狭长的蛇绿岩带为特征(图1a)。雅鲁藏布蛇绿岩带大致沿着雅鲁藏布江谷地两侧呈近东西向展布,其长度超过2500 km,是中国规模最大的蛇绿岩带之一(图1b),代表了新特提斯洋闭合后大洋岩石圈的残余(王希斌等, 1987; 张旗等, 2003)。根据雅鲁藏布蛇绿岩的地理分布及产出特征,该蛇绿岩带从东向西被划分为东段、中段和西段(王希斌等, 1987)。日喀则蛇绿岩是中段蛇绿岩的典型代表,由一系列包含不同洋壳比例的岩体组成,从西向东包括昂仁、吉定、路曲、下鲁、群让、得几、白朗、白岗、大竹曲和仁布等岩体(图1c)。前人对这些地区出露的蛇绿岩中辉长-辉绿岩开展过大量原位

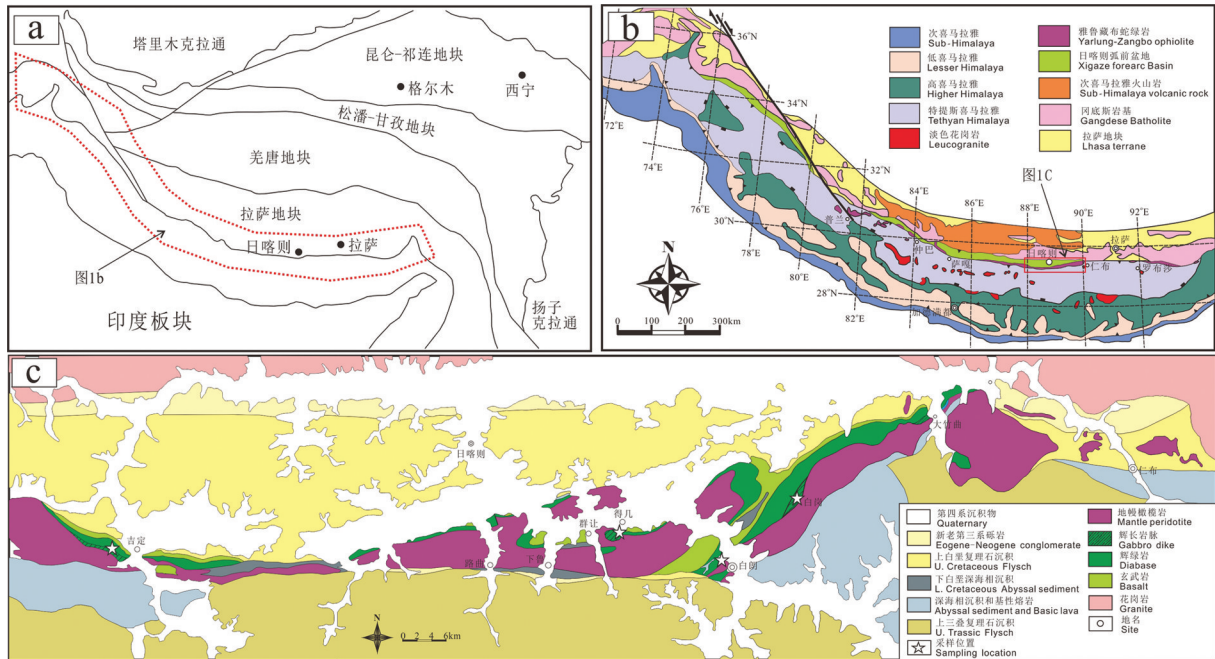


图1 雅鲁藏布蛇绿岩分布图
 a—青藏高原构造划分(据 Pan et al., 2012); b—喜马拉雅地质简图(据 An et al., 2014);
 c—日喀则蛇绿岩分布图及此次研究采样点位置(据王希斌等,1987)

Fig.1 Geological map of ophiolitic rocks of YZSZ

a—Tectonic subdivision of the Tibetan Plateau(modified from Pan et al., 2012); b—Simplified geological map of the Himalaya (modified from An et al., 2014); c—Geological map of the Xigaze ophiolite and sampling locations in this study (modified from Wang et al., 1987)

U-Pb 锆石定年工作,统计发现其形成年代分布在 131~123 Ma(吴福元等 2014)。日喀则蛇绿岩除广泛出露地幔橄辉岩外,以出露相对较完整的洋壳单元为特征,自南向北一般显示地幔橄辉岩、辉长岩-辉绿岩到玄武岩的岩相变化规律(图 1c)。日喀则蛇绿岩南侧为厚层的三叠纪嘎学群混杂堆积,与蛇绿岩断层接触,北侧为蛇绿岩逆冲到古近一新近纪日喀则组之上(王希斌等,1987)。此外,日喀则蛇绿岩南侧伴随一条与之平行分布的蛇绿岩混杂岩带,这些混杂岩主要由蛇绿岩基质和变辉绿-辉长岩(异剥钙榴岩)、石榴石角闪岩为岩块组成。

3 地质及岩相学特征

日喀则蛇绿岩的地幔橄辉岩出露面积远大于镁铁质岩石,但地幔橄辉岩大部分已经蛇纹石化,只有路曲、大竹曲和仁布等岩体仍然保存新鲜的地幔橄辉岩(图 1c)。地幔橄辉岩以方辉橄辉岩和含单斜辉石方辉橄辉岩为主,也出露一定量的二辉橄辉岩,少数岩体的地幔橄辉岩中局部含纯橄岩透镜体和豆荚状铬铁矿(余宇伟等,2017; Xiong et al., 2017)。地幔橄辉岩之上完全缺失过渡带超镁铁质

杂岩(王希斌等,1987)。日喀则蛇绿岩的辉长岩不发育,仅在吉定、白岗和大竹曲等岩体发现少量辉长岩侵入体。辉长岩多呈脉状侵入到辉绿岩中(图 2a~b),局部也可见辉长岩中包裹角砾状辉绿岩说明辉长岩侵入相对较晚(图 2c)。此外,少量辉长岩脉也侵入到下覆的地幔橄辉岩中,且这些辉长岩脉多已发生异剥钙榴岩化(图 3a)(Zhang et al., 2016; Liu et al., 2016)。日喀则地区出露的辉长岩呈两种结构类型,一种为块状,其中单斜辉石和斜长石含量大致相等(图 2a~c)。另一种辉长岩呈韵律结构(图 2d~f),多显示暗色层和浅色层交互的韵律层,矿物的粒度和条带的厚度均发生明显变化,矿物粒度变化范围从细粒到伟晶(图 2d),韵律条带厚度从几厘米到几十厘米不等(图 2e~f)。韵律层之间的矿物种类和粒度呈过渡变化,暗色层单斜辉石含量约 50%~60%,而斜长石含量为 40%~50%,当过渡到浅色层时,单斜辉石含量降低而斜长石含量增高,典型的浅色辉长岩单斜辉石含量为 35%~40%,而斜长石含量约 60%,当斜长石含量超过 90%时,可形成斜长岩条带(图 2d)。日喀则蛇绿岩的地幔橄辉岩和玄武质熔岩之间普遍发育辉绿岩,其产状主要有三

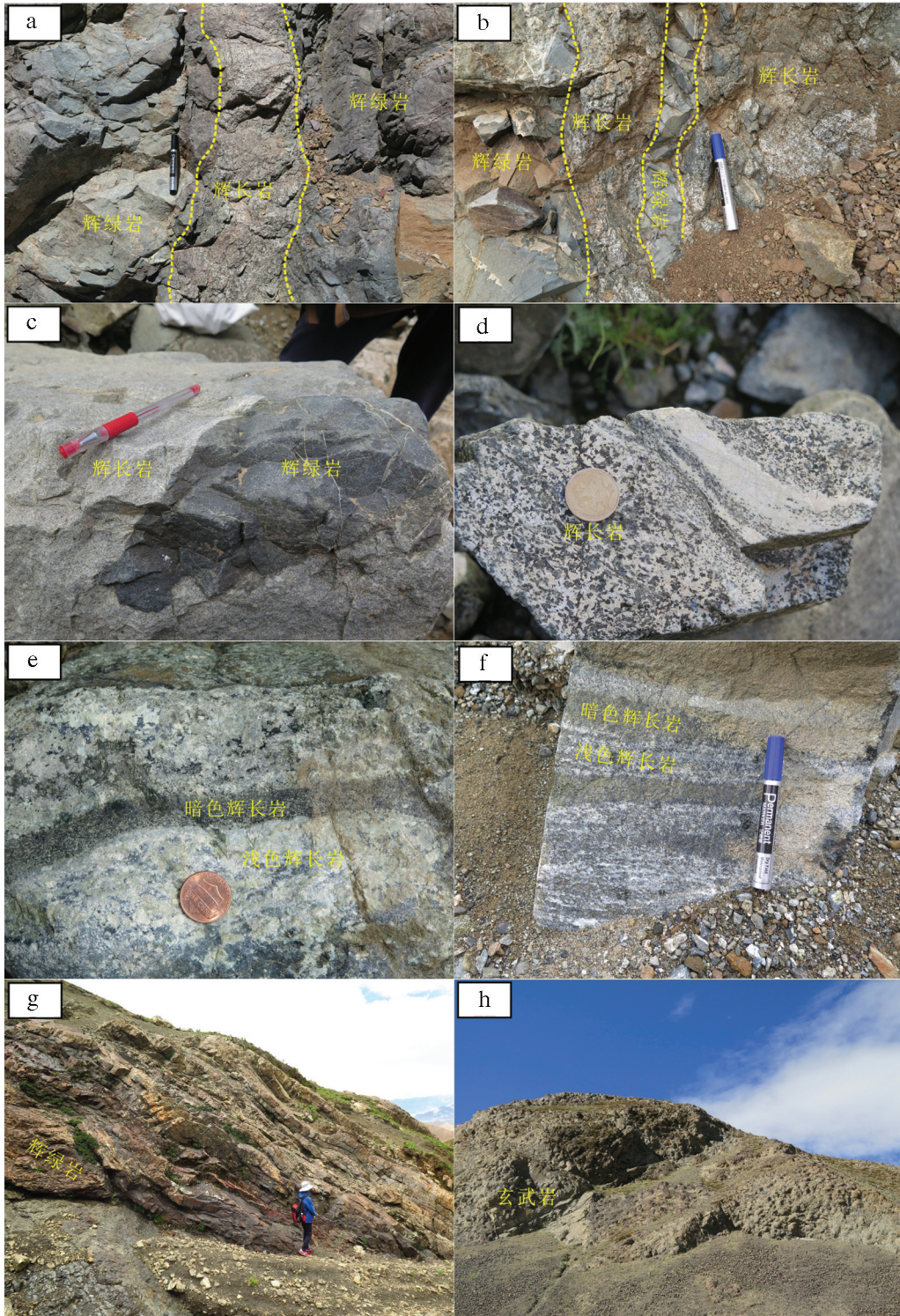


图2 日喀则蛇绿岩镁铁质岩石野外关系

a—辉长岩脉侵入辉绿岩;b—辉绿岩中不同规模的辉长岩脉;c—块状辉长岩包裹角砾状辉绿岩;d—块状粗粒辉长岩中细粒辉长岩和斜长岩;
e—辉长岩中暗色辉长岩条带;f—暗色辉长岩和浅色辉长岩互层;g—辉绿岩席;h—枕状玄武岩

Fig. 2 Field relationships of mafic rocks in the Xigaze ophiolite

a—Gabbro dikes that intruded into the diabases; b—Varying sizes of gabbro dikes in the diabases; c—Brecciated diabases enclosed by the massive gabbros; d—Fined-grained gabbro and anorthosite in the massive gabbros; e—Banded melagabbro in the gabbros; f—Rhythmic layers consisting of melagabbro and leucogabbro; g—Diabase sills; h—Pillow basalts

种类型。一种呈脉状侵入到下覆的地幔橄榄岩中(图3b),这种脉状辉绿岩与侵入到地幔橄榄岩中的脉状辉长岩产出特征类似(Nicolas et al., 1981;王希斌等, 1987; Zhang et al., 2016; Liu et al., 2016)。另一种辉绿岩呈岩席状岩床展布(图2g,图3b~f),不同于经典蛇纹岩剖面中陡直的辉绿岩墙群,这些辉绿岩席与上覆玄武岩之间不存在截然的分界,与下覆地幔橄榄岩侵入接触,呈岩席状侵入到地幔橄榄岩之上(图3d~f)。席状辉绿岩常包裹少量地幔橄榄岩捕掳体(图3c),辉绿岩席与下覆的地幔橄榄岩接触带位置靠近辉绿岩一侧常发育冷凝边(图3e)。另外,席状辉绿岩床也普遍与下覆地幔橄榄岩呈断层接触,这是在蛇纹岩构造侵位过程中造成的。辉绿岩席的厚度变化较大,局部可出露下覆的地幔橄榄岩(图3f),辉绿岩与地幔橄榄岩接触带常分布大量的辉绿岩-辉长岩侵入体(图3d)。在辉绿岩席之上为一定厚度的玄武岩(图2h),在局部缺失辉绿岩席的地区,玄武岩直接覆盖在地幔橄榄岩之上,而部分地区可见玄武岩出现在硅质岩夹层中。玄武岩和辉绿岩之间没有明显的分界,玄武岩可能作为熔岩流喷发到地表(张旗等, 2015),而席状辉

绿岩床作为浅层侵入相沿玄武质熔岩流的底部和地幔橄榄岩的岩石界面顺层侵入。

4 地球化学分析方法和结果

全岩地球化学主量元素分析在澳实分析检测(广州)有限公司完成,分析仪器为荷兰帕纳科公司生产的X荧光光谱仪,型号为PANalytical MagXFast。通过XRF射线光谱仪对制成四硼酸锂玻璃进行分析,分析精度优于5%。全岩地球化学微量元素分析在中科院地球化学研究所矿床地球化学重点实验室完成,测试仪器为Perkin-Elmer Sciex ELAN DRC-e电感耦合等离子体质谱仪(ICP-MS),分析精度优于5%。此次地球化学分析的主要岩石包括辉长岩、辉绿岩和玄武岩,其主量和微量元素分析结果见表1。

此次研究日喀则蛇纹岩的辉长岩、辉绿岩和玄武岩的烧失量分别为1.50%~4.01%、1.60%~3.53%、1.75%~4.71%。辉长岩的 $Mg^{\#}$ 除1个样品为47.0外,大部分样品介于62.7~82.8。相比而言,辉绿岩的 $Mg^{\#}$ 相对较低,除1个样品较高(70.6),其余样品分布在53.2~66.4。而玄武岩的 $Mg^{\#}$ 为42.0~59.7。日

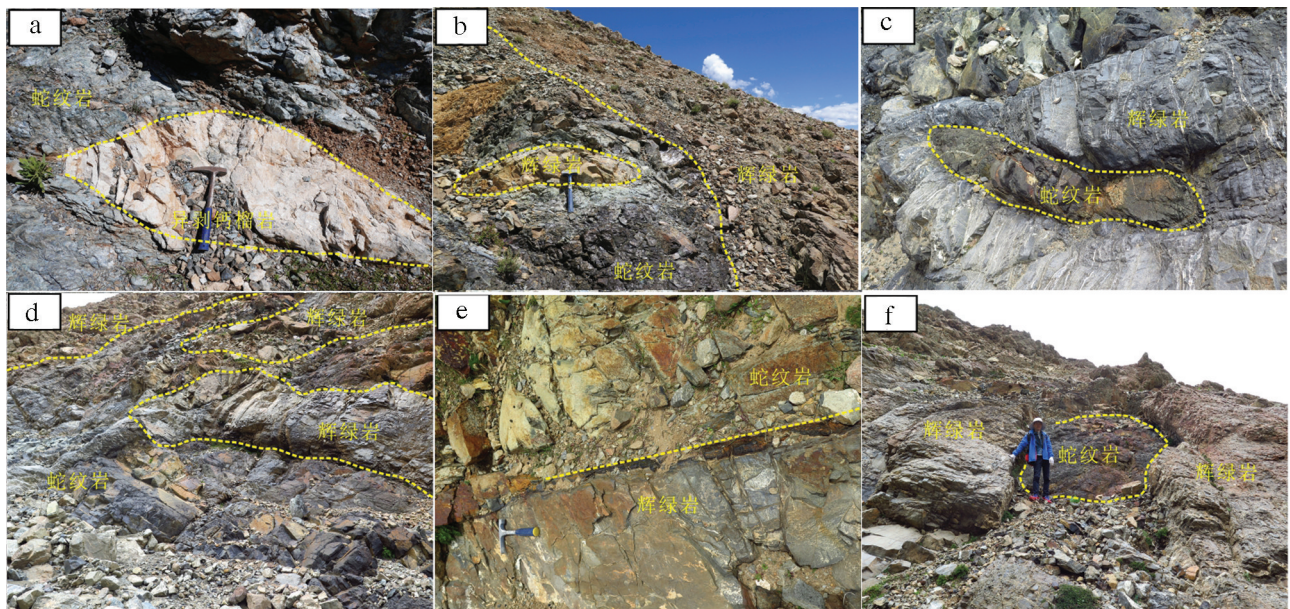


图3 日喀则蛇纹岩地幔岩石和洋壳岩石的野外照片

a—侵入到地幔橄榄岩中异剥钙榴岩脉;b—地幔橄榄岩中辉绿岩脉和辉绿岩席;c—辉绿岩中的地幔橄榄岩捕掳体;
d—辉绿岩席与地幔橄榄岩的接触带;e—发育冷凝边的辉绿岩席;f—辉绿岩席局部出露下覆地幔橄榄岩

Fig.3 Field relationships between the mantle rocks and oceanic crust rocks in the Xigaze ophiolite

a—Rodingites in the mantle peridotites; b—Diked diabases and diabase sills in the mantle peridotites; c—Xenoliths of mantle peridotites within the diabase sills; d—The boundary between the diabase sills and mantle peridotites; e—Diabase sills with chilled margins; f—The diabase sills with outcrops of the mantle peridotites

喀则蛇绿岩镁铁质岩石的 $Mg^{\#}$ 与 SiO_2 含量呈负相关关系,且大多数辉绿岩和玄武岩分布在阿曼 Geotime 和 Lasial 玄武岩的范围(图4a)。日喀则辉绿岩和玄武岩的 TiO_2 含量为0.44%~1.56%,低于大多数阿曼 Geotime 玄武岩(TiO_2 平均值为1.66%),但是高于阿曼 Lasial 玄武岩(TiO_2 平均值为0.61%),而日喀则辉长岩的 TiO_2 含量变化较大(图4b)。日喀则辉绿岩和玄武岩与阿曼 Geotime 和 Lasial 玄武岩显示相似的 Al_2O_3 和 MnO 含量,而大多数辉长岩显示更高的 Al_2O_3 和更低的 MnO 含量(图4c、d)。相似地,日喀则辉绿岩和玄武岩的 CaO 和 Na_2O 含量均落入阿曼 Geotime 和 Lasial 玄武岩的范围,而大多数辉长岩则显示较高的 CaO 和较低的 Na_2O 含量(图4e、f)。

在N-MORB标准化微量元素配分模式图中,除一个样品外,日喀则玄武岩样品之间具有相似的微量元素特征且具有Nb负异常,而其他微量元素含量均接近于N-MORB(图5a)。此外,日喀则玄武岩的微量元素含量接近阿曼 Geotimes 玄武岩,明显高于阿曼 Lasail 玄武岩,但是Nb含量相似于阿曼 Lasail 玄武岩。日喀则辉绿岩的微量元素特征与玄武岩类似,除了Nb的负异常之外,这些辉绿岩的Zr、Hf、Ti、REE等强不相容元素含量接近于N-MORB,其范围也落入阿曼 Geotimes 玄武岩的范围(图5b)。日喀则辉长岩的微量元素含量远低于N-MORB,部分样品落入阿曼 Lasail 玄武岩的范围(图5c)。

5 讨论

5.1 辉长岩的成因

经典的蛇绿岩剖面如阿曼蛇绿岩,其辉长岩位于壳幔过渡带纯橄岩和超镁铁质堆晶杂岩之上,并被上覆的辉绿岩墙群所覆盖,代表了洋壳中下部岩浆房活动的产物(Coleman, 1971)。岩浆房演化形成厚层的层状和块状辉长岩增大了洋壳的厚度,同时,岩浆房供应大量的岩浆通过辉绿岩墙群所代表的岩浆通道运移至地表形成了枕状玄武岩(Boudier and Coleman, 1981; Macleod and Yaouancq, 2000)。与阿曼蛇绿岩不同的是,日喀则蛇绿岩不发育辉长岩(Nicolas et al., 1981),仅局部出露少量呈脉状产出的辉长岩(图2),缺失厚层的层状和块状辉长岩体(图1)。日喀则辉长岩一般呈脉状侵入到辉绿岩中(图2a~b),常见辉长岩脉中包

含辉绿岩角砾(图2c),暗示辉长岩侵位时间要晚于辉绿岩。此外,可见少量辉长岩脉侵入到地幔橄橄榄岩中(图3a)(Zhang et al., 2016; Liu et al., 2016)。因此,辉长岩可能是晚期沿着辉绿岩和地幔橄橄榄岩之间的岩石界面侵入。日喀则辉长岩显示两种不同的结构特征,一种为块状结构(图2a~c),另一种显示明显的矿物韵律结构(图2d~f)。块状结构表明岩浆侵入后没有发生明显的矿物分选,岩浆在相对稳定的环境下冷凝固晶(Macleod and Yaouancq, 2000)。而呈韵律产出的辉长岩则暗示岩浆发生定向矿物分选(Irvine, 1977)。由于日喀则蛇绿岩在野外露头没有发现大规模产状连续的层状辉长岩体,因此,这些呈韵律交互结构的辉长岩有可能形成于更深部位置的小规模岩浆囊分异后形成富晶粥岩浆,这种富晶粥的岩浆在构造和热动力学的作用下侵入到上覆的岩石中并在局部发生矿物流动分选。日喀则韵律结构辉长岩中变化的矿物富集条带以及高度分选的矿物集合体的特征表明矿物经历了强烈的流动分选(图2d)。因此,日喀则蛇绿岩没有大规模原位结晶的堆晶辉长岩,即不存在稳定的岩浆房,取而代之的是少量辉长质岩浆侵入。在慢速扩张脊,由于岩浆供应量有限,一般不发育岩浆房,即不发育堆晶岩(Robinson et al., 2008)。在拆离伸展作用下,软流圈地幔上涌导致岩石圈地幔抬升到浅部位置,而软流圈地幔减压熔融形成少量岩浆聚集到地幔浅部形成小规模岩浆囊。岩浆囊的演化程度导致结晶出不同比例的矿物,这些演化的岩浆沿着岩石界面侵入形成了韵律辉长岩和块状辉长岩。因此,形成日喀则辉长岩的富晶粥岩浆可能起源于深部小规模岩浆囊分异,而非稳定的、规模较大的岩浆房。

5.2 辉绿岩的成因

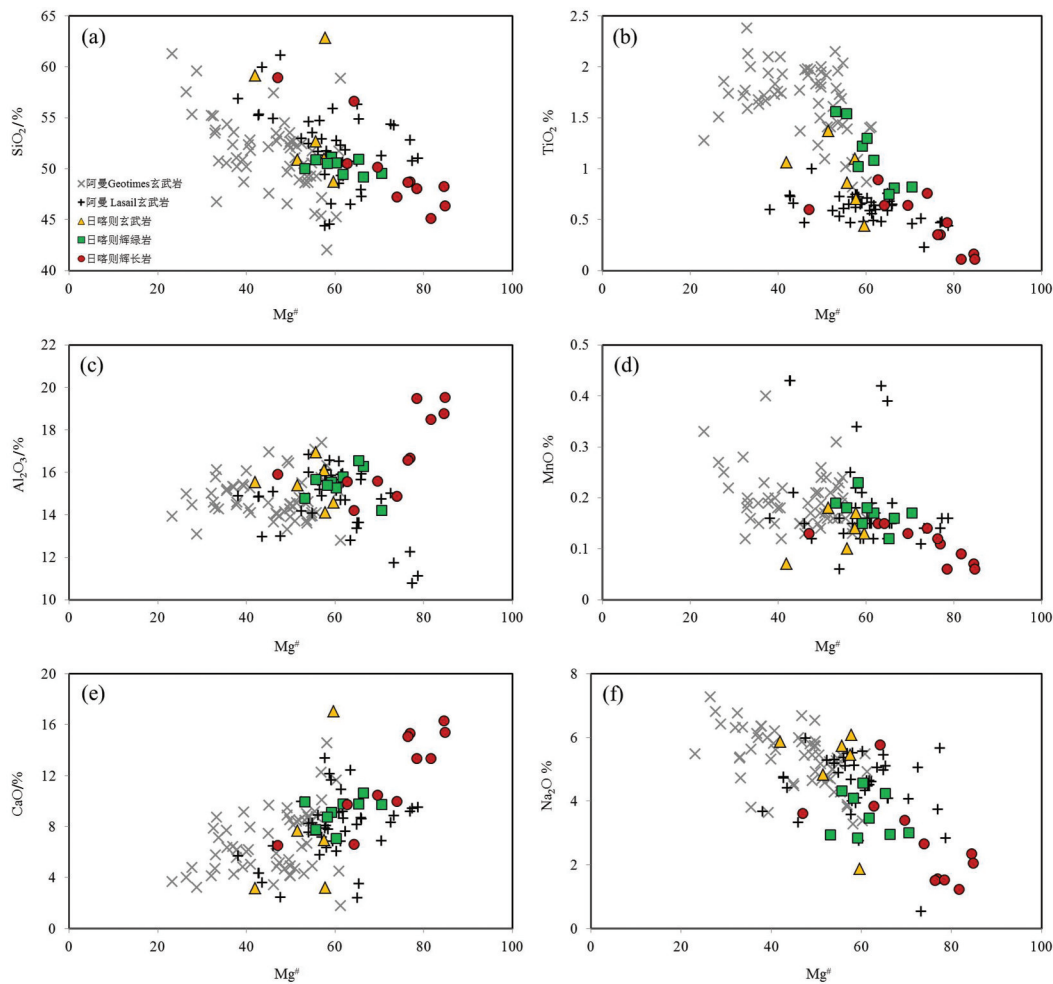
阿曼蛇绿岩的辉绿岩一般呈陡直的席状岩墙群出现,发育单向冷凝边,连接下覆的辉长岩和上部的玄武质喷出岩,代表下覆岩浆房中岩浆向上运移的通道(Coleman, 1971; Rothery, 1983)。日喀则辉绿岩相对辉长岩规模较大(图1),但不同于阿曼蛇绿岩的是日喀则蛇绿岩缺失辉绿岩墙群,取而代之的是大量的席状辉绿岩床沿着地幔橄橄榄岩的岩石边界顺层侵入(Nicolas et al., 1981; 王希斌等, 1987)。此外,少量脉状辉绿岩侵入下覆的地幔橄

表1 日喀则蛇绿岩辉长岩、辉绿岩和玄武岩全岩主量(%)和微量(10^{-6})元素成分Table 1 Compositions of whole rock major (%) and trace (10^{-6}) elements of mafic rocks from the Xigaze ophiolite

| 样品 | DJ16-19 | DJ16-23 | BL16-1 | BL16-12 | BG16-2 | BG16-3 | JD15-10 | JD15-15 | DJ16-9 | DJ16-12 | BL16-9 | BL16-20A |
|---------------------------------|---------|---------|--------|---------|--------|--------|---------|---------|--------|---------|--------|----------|
| 岩性 | 玄武岩 | 玄武岩 | 玄武岩 | 玄武岩 | 玄武岩 | 玄武岩 | 辉绿岩 | 辉绿岩 | 辉绿岩 | 辉绿岩 | 辉绿岩 | 辉绿岩 |
| SiO ₂ | 48.7 | 59.2 | 50.9 | 62.9 | 51.0 | 52.7 | 50.0 | 51.1 | 49.5 | 49.2 | 50.6 | 50.9 |
| TiO ₂ | 0.44 | 1.06 | 1.37 | 0.70 | 1.10 | 0.86 | 1.56 | 1.22 | 1.08 | 0.81 | 1.30 | 1.54 |
| Al ₂ O ₃ | 14.6 | 15.6 | 15.4 | 14.1 | 16.1 | 16.9 | 14.8 | 15.5 | 15.8 | 16.3 | 15.3 | 15.7 |
| Cr ₂ O ₃ | 0.05 | 0.01 | 0.01 | 0.01 | 0.03 | 0.02 | 0.02 | 0.02 | 0.04 | 0.05 | 0.01 | 0.03 |
| TFe ₂ O ₃ | 7.1 | 8.95 | 10.75 | 6.65 | 9.41 | 7.95 | 11.54 | 9.30 | 9.27 | 8.08 | 10.3 | 10.7 |
| MnO | 0.13 | 0.07 | 0.18 | 0.17 | 0.14 | 0.1 | 0.19 | 0.15 | 0.17 | 0.16 | 0.18 | 0.18 |
| MgO | 5.25 | 3.24 | 5.71 | 4.55 | 6.38 | 5 | 6.55 | 6.74 | 7.49 | 8 | 7.79 | 6.71 |
| CaO | 17.1 | 3.13 | 7.67 | 3.2 | 6.92 | 7.74 | 9.92 | 9.09 | 9.75 | 10.7 | 7.04 | 7.77 |
| Na ₂ O | 1.87 | 5.87 | 4.83 | 6.07 | 5.45 | 5.73 | 2.93 | 2.83 | 3.46 | 2.96 | 4.56 | 4.32 |
| K ₂ O | 0.01 | 0.05 | 0.03 | 0.11 | 0.21 | 0.07 | 0.11 | 0.82 | 0.19 | 0.17 | 0.18 | 0.13 |
| LOI | 4.71 | 2.97 | 2.64 | 1.75 | 3.35 | 2.96 | 1.60 | 2.99 | 3.13 | 3.53 | 2.84 | 2.53 |
| Total | 99.9 | 100.1 | 99.4 | 100.2 | 100.1 | 100.1 | 99.2 | 99.8 | 99.8 | 99.9 | 100.0 | 100.4 |
| Mg# | 59.7 | 42.0 | 51.5 | 57.8 | 57.6 | 55.7 | 53.2 | 59.2 | 61.8 | 66.4 | 60.3 | 55.7 |
| V | 221 | 215 | 301 | 134 | 278 | 257 | 306 | 285 | 250 | 201 | 270 | 303 |
| Cr | 330 | 10.0 | 40.0 | 70.0 | 190 | 120 | 148 | 153 | 290 | 290 | 90 | 170 |
| Ga | 21.7 | 16.6 | 16.3 | 10.8 | 15.0 | 16.3 | 17.3 | 15.7 | 14.7 | 12.9 | 14.4 | 14.6 |
| Rb | 0.20 | 0.30 | 0.20 | 0.50 | 1.90 | 0.60 | 0.68 | 4.96 | 1.40 | 1.20 | 0.90 | 0.40 |
| Sr | 35.1 | 66.5 | 158 | 67 | 250 | 81 | 144 | 129 | 229 | 211 | 135 | 389 |
| Y | 12.3 | 38.2 | 29.0 | 36.0 | 25.0 | 20.0 | 33.0 | 25.3 | 25.3 | 17.4 | 27.1 | 25.8 |
| Zr | 30.0 | 118.0 | 85.0 | 129.0 | 77.0 | 60.0 | 103.0 | 74.0 | 64.0 | 51.0 | 85.0 | 72.0 |
| Nb | 0.20 | 1.10 | 0.80 | 1.10 | 1.00 | 0.60 | 1.38 | 1.06 | 0.50 | 0.40 | 0.90 | 0.70 |
| Ba | 6.10 | 7.80 | 8.30 | 4.50 | 19.60 | 14.00 | 5.63 | 15.40 | 8.50 | 6.50 | 9.30 | 10.20 |
| La | 1.10 | 3.90 | 2.70 | 3.70 | 2.10 | 2.00 | 3.52 | 2.56 | 2.10 | 1.70 | 3.00 | 2.50 |
| Ce | 3.40 | 12.30 | 8.90 | 11.50 | 7.00 | 5.90 | 11.60 | 8.49 | 6.70 | 5.40 | 9.40 | 7.80 |
| Pr | 0.57 | 1.93 | 1.49 | 1.96 | 1.16 | 1.03 | 1.85 | 1.37 | 1.21 | 0.93 | 1.58 | 1.32 |
| Nd | 2.90 | 10.00 | 7.90 | 10.40 | 6.80 | 5.60 | 10.50 | 7.67 | 6.80 | 5.00 | 7.90 | 7.20 |
| Sm | 1.00 | 3.65 | 2.98 | 3.56 | 2.43 | 2.11 | 3.36 | 2.49 | 2.61 | 1.80 | 2.94 | 2.64 |
| Eu | 0.42 | 1.30 | 1.12 | 0.77 | 1.00 | 0.90 | 1.37 | 1.02 | 1.00 | 0.70 | 1.10 | 0.88 |
| Gd | 1.55 | 4.98 | 4.10 | 4.65 | 3.88 | 2.95 | 4.47 | 3.21 | 3.66 | 2.68 | 4.17 | 3.68 |
| Tb | 0.29 | 0.89 | 0.73 | 0.85 | 0.65 | 0.54 | 0.84 | 0.60 | 0.64 | 0.44 | 0.65 | 0.64 |
| Dy | 1.92 | 6.28 | 4.87 | 5.59 | 4.39 | 3.55 | 5.62 | 4.21 | 4.23 | 2.73 | 4.46 | 4.36 |
| Ho | 0.42 | 1.41 | 1.09 | 1.29 | 0.95 | 0.77 | 1.30 | 0.96 | 0.92 | 0.62 | 1.03 | 0.97 |
| Er | 1.22 | 4.07 | 3.07 | 3.78 | 2.68 | 2.24 | 3.54 | 2.78 | 2.48 | 1.86 | 2.76 | 2.71 |
| Tm | 0.18 | 0.60 | 0.47 | 0.59 | 0.38 | 0.33 | 0.51 | 0.41 | 0.36 | 0.24 | 0.42 | 0.43 |
| Yb | 1.13 | 4.03 | 3.02 | 3.79 | 2.46 | 2.14 | 3.35 | 2.59 | 2.34 | 1.74 | 2.49 | 2.74 |
| Lu | 0.17 | 0.62 | 0.45 | 0.59 | 0.39 | 0.33 | 0.52 | 0.39 | 0.36 | 0.28 | 0.41 | 0.41 |
| Hf | 0.90 | 3.50 | 2.60 | 3.90 | 2.20 | 1.70 | 2.57 | 1.94 | 2.00 | 1.60 | 2.40 | 2.10 |
| Ta | 0.07 | 0.11 | 0.09 | 0.09 | 0.10 | 0.08 | 0.10 | 0.08 | 0.10 | 0.09 | 0.07 | 0.06 |
| Th | 0.05 | 0.18 | 0.10 | 0.17 | 0.09 | 0.09 | 0.10 | 0.07 | 0.07 | 0.08 | 0.10 | 0.06 |

续表1

| BG16- 8 | BG16- 9 | BG15- 16 | JD15- 12 | JD15- 13 | DJ16- 6 | DJ16- 15 | BL16- 20B | BL16- 21 | BG15- 9 | BG15- 11 | BG15- 12 | BG16- 14 | BG16- 15 |
|------------|------------|-------------|-------------|-------------|------------|-------------|--------------|-------------|------------|-------------|-------------|-------------|-------------|
| 辉绿岩 | 辉绿岩 | 辉绿岩 | 辉长岩 | 辉长岩 | 辉长岩 | 辉长岩 | 辉长岩 | 辉长岩 | 辉长岩 | 辉长岩 | 辉长岩 | 辉长岩 | 辉长岩 |
| 49.6 | 50.5 | 50.9 | 48.7 | 48.7 | 48.0 | 58.9 | 50.5 | 50.1 | 45.1 | 48.3 | 46.4 | 56.6 | 47.2 |
| 0.82 | 1.02 | 0.75 | 0.35 | 0.35 | 0.47 | 0.60 | 0.89 | 0.64 | 0.11 | 0.16 | 0.11 | 0.64 | 0.76 |
| 14.2 | 15.4 | 16.6 | 16.7 | 16.6 | 19.5 | 15.9 | 15.6 | 15.6 | 18.5 | 18.8 | 19.5 | 14.2 | 14.9 |
| 0.09 | 0.02 | 0.05 | 0.13 | 0.12 | 0.09 | 0.01 | 0.03 | 0.06 | 0.10 | 0.13 | 0.13 | 0.03 | 0.1 |
| 8.72 | 9.99 | 7.33 | 5.61 | 6.00 | 4.21 | 8 | 8.68 | 7.44 | 5.63 | 3.00 | 3.18 | 7.24 | 8.25 |
| 0.17 | 0.23 | 0.12 | 0.11 | 0.12 | 0.06 | 0.13 | 0.15 | 0.13 | 0.09 | 0.07 | 0.06 | 0.15 | 0.14 |
| 10.5 | 6.98 | 6.90 | 9.34 | 9.71 | 7.67 | 3.55 | 7.31 | 8.51 | 12.6 | 8.20 | 8.89 | 6.5 | 11.7 |
| 9.71 | 8.76 | 9.75 | 15.3 | 15.1 | 13.4 | 6.51 | 9.73 | 10.5 | 13.4 | 16.3 | 15.4 | 6.62 | 9.98 |
| 3.01 | 4.09 | 4.24 | 1.55 | 1.50 | 1.52 | 3.61 | 3.84 | 3.4 | 1.22 | 2.34 | 2.05 | 5.77 | 2.66 |
| 0.27 | 0.02 | 0.40 | 0.27 | 0.30 | 1.56 | 0.27 | 0.06 | 0.14 | 0.08 | 0.09 | 0.10 | 0.21 | 0.64 |
| 3.14 | 3.02 | 2.88 | 2.02 | 1.97 | 4.19 | 1.72 | 2.94 | 2.93 | 3.34 | 2.98 | 4.01 | 1.5 | 3.67 |
| 100.1 | 100.0 | 99.9 | 100.1 | 100.4 | 100.6 | 99.3 | 99.7 | 99.4 | 100.1 | 100.3 | 99.8 | 99.5 | 100.0 |
| 70.6 | 58.3 | 65.3 | 76.9 | 76.4 | 78.5 | 47.0 | 62.7 | 69.6 | 81.7 | 84.5 | 84.8 | 64.2 | 73.9 |
| 204 | 260 | 207 | 191 | 184 | 131 | 212 | 230 | 205 | 92 | 163 | 106 | 209 | 183 |
| 620 | 130 | 249 | 800 | 801 | 640 | 20.0 | 220 | 400 | 726 | 946 | 810 | 180 | 620 |
| 13.3 | 15.3 | 14.6 | 12.0 | 11.5 | 11.9 | 14.4 | 13.3 | 14.5 | 10.6 | 10.3 | 11.1 | 9.2 | 11.5 |
| 1.50 | 0.20 | 1.64 | 2.82 | 3.71 | 16.00 | 2.20 | 0.40 | 0.50 | 0.71 | 0.67 | 0.89 | 1.00 | 2.60 |
| 221 | 149 | 280 | 153 | 154 | 329 | 124 | 141 | 310 | 150 | 239 | 208 | 198 | 122 |
| 17.5 | 23.7 | 16.0 | 10.3 | 10.2 | 10.1 | 23.5 | 20.3 | 14.6 | 3.0 | 5.9 | 3.5 | 15.2 | 15.5 |
| 50.0 | 64.0 | 44.7 | 11.5 | 12.5 | 19.0 | 61.0 | 65.0 | 39.0 | 1.8 | 3.1 | 1.9 | 37.0 | 45.0 |
| 0.60 | 0.60 | 0.43 | 0.05 | 0.05 | 0.20 | 0.40 | 1.10 | 0.50 | 0.02 | 0.02 | 0.02 | 0.30 | 0.50 |
| 12.60 | 3.90 | 10.20 | 3.09 | 7.25 | 160.50 | 18.00 | 5.80 | 9.60 | 1.21 | 2.07 | 7.36 | 6.40 | 8.60 |
| 1.50 | 1.90 | 1.27 | 0.49 | 0.44 | 1.00 | 4.40 | 2.30 | 1.70 | 0.12 | 0.13 | 0.18 | 1.30 | 1.90 |
| 5.00 | 6.40 | 4.38 | 1.78 | 1.94 | 3.10 | 9.70 | 7.00 | 4.90 | 0.39 | 0.54 | 0.34 | 4.10 | 5.60 |
| 0.89 | 1.13 | 0.70 | 0.32 | 0.36 | 0.52 | 1.00 | 1.22 | 0.75 | 0.07 | 0.11 | 0.08 | 0.72 | 0.90 |
| 4.80 | 6.30 | 4.04 | 1.87 | 2.14 | 2.60 | 5.30 | 6.60 | 4.20 | 0.44 | 0.79 | 0.48 | 4.00 | 5.30 |
| 1.73 | 2.40 | 1.31 | 0.93 | 0.82 | 0.95 | 1.99 | 2.41 | 1.60 | 0.17 | 0.43 | 0.23 | 1.44 | 1.82 |
| 0.73 | 0.92 | 0.61 | 0.49 | 0.50 | 0.44 | 0.61 | 0.99 | 0.61 | 0.17 | 0.25 | 0.25 | 0.55 | 0.78 |
| 2.79 | 3.38 | 1.79 | 1.24 | 1.43 | 1.36 | 2.88 | 2.98 | 2.20 | 0.33 | 0.62 | 0.36 | 2.20 | 2.60 |
| 0.44 | 0.64 | 0.33 | 0.25 | 0.23 | 0.24 | 0.57 | 0.58 | 0.39 | 0.06 | 0.12 | 0.07 | 0.43 | 0.46 |
| 3.09 | 4.23 | 2.39 | 1.77 | 1.77 | 1.58 | 3.75 | 3.76 | 2.64 | 0.47 | 0.85 | 0.57 | 2.78 | 2.87 |
| 0.66 | 0.91 | 0.58 | 0.37 | 0.41 | 0.34 | 0.88 | 0.82 | 0.58 | 0.09 | 0.21 | 0.15 | 0.61 | 0.64 |
| 1.96 | 2.52 | 1.50 | 1.07 | 1.13 | 0.94 | 2.59 | 2.37 | 1.66 | 0.22 | 0.63 | 0.36 | 1.74 | 1.78 |
| 0.30 | 0.36 | 0.21 | 0.15 | 0.16 | 0.14 | 0.41 | 0.34 | 0.24 | 0.04 | 0.07 | 0.05 | 0.26 | 0.27 |
| 1.81 | 2.40 | 1.45 | 0.95 | 0.94 | 0.86 | 2.65 | 2.24 | 1.54 | 0.25 | 0.47 | 0.34 | 1.67 | 1.69 |
| 0.27 | 0.37 | 0.22 | 0.15 | 0.14 | 0.13 | 0.40 | 0.35 | 0.24 | 0.04 | 0.07 | 0.05 | 0.24 | 0.25 |
| 1.30 | 1.90 | 1.04 | 0.34 | 0.36 | 0.60 | 1.90 | 1.70 | 1.20 | 0.08 | 0.19 | 0.07 | 1.30 | 1.30 |
| 0.07 | 0.05 | 0.04 | 0.00 | 0.00 | 0.01 | 0.03 | 0.02 | 0.02 | 0.00 | 0.01 | 0.00 | 0.00 | 0.01 |
| 0.06 | 0.07 | 0.04 | 0.01 | 0.01 | 0.06 | 0.10 | 0.09 | 0.23 | 0.01 | 0.01 | 0.00 | 0.12 | 0.08 |

图4 日喀则蛇绿岩全岩 $Mg^{\#}$ 与主量元素相关图Fig.4 Correlations of whole-rock $Mg^{\#}$ with major elements of the Xigaze ophiolitic rocks

榄岩中(图3)。这些侵入到下覆地幔橄榄岩中的辉绿岩脉与侵入到地幔橄榄岩中的脉状辉长岩产出特征类似(图3a~b),暗示这类辉绿岩的侵入时间和机制可能与辉长岩脉相似(Nicolas et al., 1981; 王希斌等, 1987; Zhang et al., 2016; Liu et al., 2016)。而另一类辉绿岩呈岩席状岩床展布且直接与地幔橄榄岩侵入接触(图3b~f),这些辉绿岩席中常包裹已蛇纹石化的地幔橄榄岩包体(图3c),说明辉绿岩席与地幔橄榄岩之间不存在辉长岩体。值得注意的是,在辉绿岩席一侧发育冷凝边(图3e),这说明当辉绿岩席侵入时,其下覆的地幔橄榄岩体已经抬升到较浅的位置并快速冷凝。日喀则辉绿岩席的厚度变化较大(图3d,f),这表明来自深部的岩浆供应是高度变化的,不同规模的基性岩浆沿岩石界面迁移并侵入到地幔橄榄岩之上形成了辉绿岩席。阿

曼蛇绿岩的辉绿岩墙群是岩浆沿着由张力作用形成的断层侵入的结果,一般形成于洋脊扩张环境下(Rothery, 1983; Nicolas et al., 1994; Macleod and Yaouancq, 2000)。然而,日喀则蛇绿岩的辉绿岩席沿地幔橄榄岩界面侵入,拆离断层可能扮演一个重要的角色(Liu et al., 2014)。在慢速—超慢速的扩张中心,拆离断层活动导致上地幔抬升至浅部并引起软流圈地幔减压部分熔融,基性岩浆沿着拆离断层形成的构造薄弱面呈岩席状侵入,由于岩浆供应量有限,岩浆侵入可能是不连续的。

5.3 日喀则蛇绿岩的成因类型及构造环境

Dilek and Furnes (2011)根据蛇绿岩的地球化学特征、内部结构、厚度、扩张速率、与地幔柱和海沟的关系、地幔的温度和富集程度等指标把蛇绿岩划分为:大陆边缘型、洋中脊型、地幔柱型、俯冲带型、

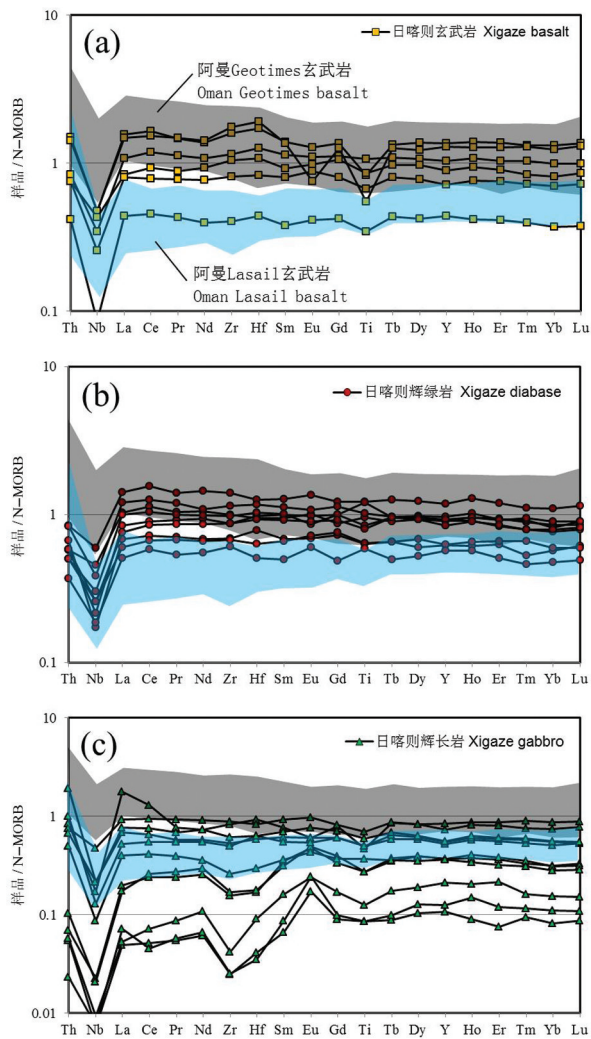


图5 全岩N-MORB标准化微量元素配分模式图
N-MORB标准化值据 Sun and McDonough, 1989; 阿曼蛇绿岩中 Geotime 和 Lasail 玄武岩数据源于 Einaudi et al., 2000; Godard et al., 2003, 2006; Kusano et al., 2013
Fig.5 N-MORB normalized trace elements patterns
Normalized values of N-MORB are from Sun and McDonough, 1989; the Geotime and Lasail basalts after Einaudi et al., 2000; Godard et al., 2003, 2006; Kusano et al., 2013

火山弧型。在洋中脊环境下,软流圈上涌导致上地幔的减压熔融产生了 MORB 性质的熔体和洋壳。阿曼蛇绿岩的 Geotimes 玄武岩显示 MORB 特征(图 5)(Godard et al., 2003, 2006),结合阿曼蛇绿岩发育大规模的岩浆房和辉绿岩墙群,阿曼蛇绿岩被认为形成于洋中脊扩张环境(Nicolas et al., 1994; Godard et al., 2006; Goodenough et al., 2014)。当阿曼蛇绿岩随板块汇聚到俯冲带,由于俯冲板片脱水 and 熔融以及俯冲物质加入,熔融的岩浆高度亏损

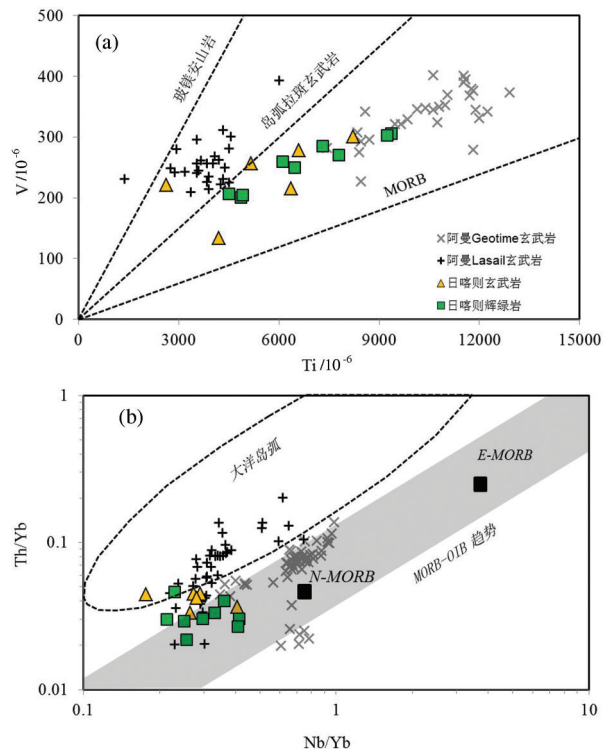


图6 微量元素构造环境判别图
a—V-Ti据 Pearce(2014); b—Nb/Yb-Th/Yb据 Pearce(2008)
Fig.6 Discriminant diagrams of tectonic settings
a—V versus Ti (after Pearce, 2000); b—Nb/Yb versus Th/Yb(after Pearce, 2008)

Nb、Ta、Zr、Hf、Ti、LREE 等不相容元素(Pearce et al., 2008, 2014),这些高度亏损不相容元素的岩浆叠加蛇绿岩之上形成了阿曼 Lasail 玄武岩(图 5)(Einaudi et al., 2000; Godard et al., 2003, 2006; Kusano et al., 2013)。此外,由于岩浆的供应与扩张的平衡被打破导致缺失辉长岩和席状岩墙群(Robinson et al., 2008)。

对于日喀则蛇绿岩而言,玄武岩和辉绿岩的微量元素模式非常相似于阿曼 Geotimes 玄武岩(图 5a、b)。根据微量元素构造判别图显示日喀则辉绿岩和玄武岩落入 MORB 环境(图 6a、b)。不同于阿曼岩体的是,日喀则镁铁质岩石形成于一个慢速的扩张脊,岩浆供应量非常有限,且地幔源区可能经历了多次不连续部分熔融并导致日喀则辉绿岩和玄武岩显示相对较低的 Ti 含量和 Th/Yb 和 Nb/Yb 比值(图 6a、b)。结合日喀则辉长岩和辉绿岩的成因可以推断,在洋中脊环境下,由于拆离断层的作用引起洋壳逐渐减薄和软流圈地幔上涌,进而导致大洋岩石圈地幔剥露和后期 MORB 质岩浆侵入形成

岩席和岩脉,由于岩浆供应的不足,在壳幔过渡带边界没有形成过渡带纯橄岩和超镁铁质堆晶岩,也没有形成大型的岩浆房和辉绿岩墙群。

6 结 论

日喀则蛇绿岩少量辉长岩脉侵入到辉绿岩和地幔橄辉岩中反映这些辉长岩脉并非岩浆房原位结晶分异的产物,而是深部位置岩浆囊中岩浆发生不同程度分异并侵入到地幔橄辉岩和辉绿岩中。辉绿岩席则是岩浆沿着构造薄弱界面呈岩席状侵入的结果,而辉绿岩脉成因与辉长岩成因类似。结合这些岩石的野外和地球化学特征暗示日喀则蛇绿岩形成于慢速扩张脊。而拆离断层作用可能导致了岩石圈地幔抬升并剥露,进而引起了不连续的软流圈地幔减压熔融和岩浆上侵。

References

An W, Hu X, Garzanti E, BouDagher-Fadel M K, Wang J, Sun G. 2014. Xigaze forearc basin revisited (South Tibet): Provenance changes and origin of the Xigaze ophiolite [J]. *Geological Society of America Bulletin*, 126: 1595–1613.

Aitchison J C, Badengzhub Davisa A M, Liua J, Luoa H, Malpasa J G, Mcdermida I R C, Wub H, Ziabreva S V, Zhou M F. 2000. Remnants of a Cretaceous intra-oceanic subduction system within the Yarlung-Zangbo suture (southern Tibet) [J]. *Earth and Planetary Science Letters*, 183: 231–244.

Alabaster T, Pearce J A, Malpas J. 1982. The volcanic stratigraphy and petrogenesis of the Oman ophiolite complex [J]. *Contributions to Mineralogy and Petrology*, 81: 168–183.

Bédard É, Hébert R, Guilmette C, Lesage G, Wang C, Dostal J. 2009. Petrology and geochemistry of the Saga and Sangsang ophiolitic massifs, Yarlung Zangbo Suture Zone, Southern Tibet: Evidence for an arc-back-arc origin [J]. *Lithos*, 113: 48–67.

Boudier F, Coleman R G. 1981. Cross section through the peridotite in the Samail ophiolite, southeastern Oman Mountains [J]. *Journal of Geophysical Research Atmospheres*, 86: 2573–2592.

Chen Genwe, Liu Rui, Xia Bin, Deng Teng. 2015. Geochemistry of the Jiding ophiolite in SW Tibet and its tectonic implications [J]. *Acta Petrologica Sinica*, 31: 2495–2507 (in Chinese with English abstract).

Coleman R G. 1971. Plate tectonic emplacement of upper mantle peridotites along continental edges [J]. *Journal of Geophysical Research*, 76: 1212–1222.

Coleman R G. 1977. Ophiolites: Ancient Oceanic Lithosphere? [M] New York: Springer-Verlag.

Dai J, Wang C, Li Y. 2012. Relicts of the Early Cretaceous seamounts in the central-western Yarlung Zangbo Suture Zone, southern

Tibet [J]. *Journal of Asian Earth Sciences*, 53: 25–37.

Dai J, Wang C, Polat A, Santosh M, Li Y, Ge Y. 2013. Rapid forearc spreading between 130 and 120 Ma: Evidence from geochronology and geochemistry of the Xigaze ophiolite, southern Tibet [J]. *Lithos*, 172: 1–16.

Dewey J F, Bird J M. 1971. Origin and emplacement of the ophiolite suite: Appalachian ophiolites in Newfoundland [J]. *Journal of Geophysical Research Atmospheres*, 76: 3179–3206.

Dilek Y, Furnes H. 2011. Ophiolite genesis and global tectonics: Geochemical and tectonic fingerprinting of ancient oceanic lithosphere [J]. *Geological Society of America Bulletin*, 123: 387–411.

Dubois-Côté V, Hébert R, Dupuis C, Wang C, Li Y, Dostal J. 2005. Petrological and geochemical evidence for the origin of the Yarlung Zangbo ophiolites, southern Tibet [J]. *Chemical Geology*, 214: 265–286.

Einaudi F, Pezard P A, Cocheme J J, Coulon C, Laverne C, Godard M. 2000. Petrography, geochemistry and physical properties of a continuous extrusive section from the Sarami Massif, Semail ophiolite [J]. *Marine Geophysical Researches*, 21: 387–407.

Girardeau J, Mercier J, Yougong Z. 1985. Structure of the Xigaze ophiolite, Yarlung Zangbo suture zone, southern Tibet, China: Genetic implications [J]. *Tectonics*, 4: 267–288.

Godard M, Bosch D, Einaudi F. 2006. A MORB source for low-Ti magmatism in the Semail ophiolite [J]. *Chemical Geology*, 234: 58–78.

Godard M, Dautria J M, Perrin M. 2003. Geochemical variability of the Oman ophiolite lavas: Relationship with spatial distribution and paleomagnetic directions [J]. *Geochemistry Geophysics Geosystems*, 4: 1–15.

Goodenough K M, Thomas R J, Styles M T, Schofield D I, MacLeod C J. 2014. Records of ocean growth and destruction in the Oman-UAE Ophiolite [J]. *Elements*, 10: 109–114.

Guilmette C, Hébert R, Wang C, Villeneuve M. 2009. Geochemistry and geochronology of the metamorphic sole underlying the Xigaze ophiolite, Yarlung Zangbo Suture Zone, south Tibet [J]. *Lithos*, 112: 149–162.

Hébert R, Bezard R, Guilmette C, Dostal J, Wang C, Liu Z. 2012. The Indus-Yarlung Zangbo ophiolites from Nanga Parbat to Namche Barwa syntaxes, southern Tibet: First synthesis of petrology, geochemistry, and geochronology with incidences on geodynamic reconstructions of Neo-Tethys [J]. *Gondwana Research*, 22: 377–397.

Irvine T N. 1977. Origin of chromite layers in the Muskox intrusion and other intrusions: A new interpretation [J]. *Geology*, 5: 273–277.

Kusano Y, Adachi Y, Miyashita S, Umino S. 2013. Lava accretion system around mid-ocean ridges: Volcanic stratigraphy in the Wadi Fizeh area, northern Oman ophiolite [J]. *Geochemistry Geophysics Geosystems*, 13: 1–25.

Li Wenxia, Zhao Zhidan, Zhu Dicheng, Dong Guochen, Zhou Shu, Mo Xuanxue, DePaolo D J, Dilek Y. 2012. Geochemical discrimination of tectonic environments of the Yarlung Zangbo ophiolite in southern Tibet [J]. *Acta Petrologica Sinica*, 28: 1663–1673 (in

- Chinese with English abstract).
- Liu C Z, Zhang C, Yang L Y, Zhang L L, Ji W Q, Wu F Y. 2014. Formation of gabbro-norites in the Purang ophiolite (SW Tibet) through melting of hydrothermally altered mantle along a detachment fault [J]. *Lithos*, 205: 127–141.
- Liu T, Wu F Y, Zhang L L, Zhai Q G, Liu C Z, Ji W B, Zhang C, Xu Y. 2016. Zircon U–Pb geochronological constraints on rapid exhumation of the mantle peridotite of the Xigaze ophiolite, southern Tibet [J]. *Chemical Geology*, 443: 67–86.
- Miyashiro A. 1973. The Troodos ophiolitic complex was probably formed in an island arc [J]. *Earth and Planetary Science Letters*, 19: 218–224.
- Macleod C J, Yaouancq G. 2000. A fossil melt lens in the Oman ophiolite: Implications for magma chamber processes at fast spreading ridges [J]. *Earth and Planetary Science Letters*, 176: 357–373.
- Nicolas A, Boudier F, Ildefonse B. 1994. Evidence from the Oman ophiolite for active mantle upwelling beneath a fast-spreading ridge [J]. *Nature*, 370: 51–53.
- Nicolas A, Girardeau J, Marcoux J, Dupre B, Xibin W, Yougong C, Haixiang Z, Xuchang X. 1981. The Xigaze ophiolite (Tibet): A peculiar oceanic lithosphere [J]. *Nature*, 294: 414–417.
- Niu Xialu, Zhao Zhidan, Mo Xuanxue, DePaolo D J, Dong Guochen, Zhang Shuangquan, Zhu Dicheng, Guo Tieying. 2006. Elemental and Sr–Nd–Pb isotopic geochemistry for basic rocks from Decun–Angren ophiolites in Xigaze area, Tibet: implications for the characteristics of the Tethyan upper mantle domain [J]. *Acta Petrologica Sinica*, 22: 2875–2888 (in Chinese with English abstract).
- Pan Guitang, Li Xinzhen, Wang Liquan, Ding Jun, Chen Zhiliang. 2002. Preliminary division of tectonic units of the Qinghai–Tibet Plateau and its adjacent regions [J]. *Geological Bulletin of China*, 21: 701–707 (in Chinese with English abstract).
- Pan G, Wang L, Li R, Yuan S, Ji W, Yin F, Zhang W, Wang B. 2012. Tectonic evolution of the Qinghai–Tibet plateau [J]. *Journal of Asian Earth Science*, 53: 3–14.
- Pearce J A. 1975. Basalt geochemistry used to investigate past tectonic environments on Cyprus [J]. *Tectonophysics*, 25: 41–67.
- Pearce J A. 2008. Geochemical fingerprinting of oceanic basalts with applications to ophiolite classification and the search for Archean oceanic crust [J]. *Lithos*, 100: 14–48.
- Pearce J A. 2014. Immobile Element Fingerprinting of Ophiolites [J]. *Elements*, 10: 101–108.
- Pearce J A, Barker P, Edwards S, Parkinson I J, Leat P. 2000. Geochemistry and tectonic significance of peridotites from the South Sandwich arc–basin system, South Atlantic [J]. *Contribution to Mineralogy and Petrology*, 139: 36–53.
- Robinson P T, Malpas J, Dilek Y, Zhou M F. 2008. The significance of sheeted dike complexes in ophiolites [J]. *GSA Today*, 18: 4–10.
- Rothery D A. 1983. The base of a sheeted dyke complex, Oman ophiolite: Implications for magma chambers at oceanic spreading axes [J]. *Journal of the Geological Society*, 140: 287–296.
- She Yuwei, Zhu Xiangkun, He Yuan, Ma Jianxiang, Sun Jian. 2017. The new discovery of the podiform chromitite in the Xigaze ophiolite, Yarlung Zangbo suture zone, Tibet [J]. *Geology in China*, 44: 610–611 (in Chinese with English abstract).
- Sun S S, McDonough W. 1989. Chemical and isotopic systematics of oceanic basalts: Implications for mantle composition and processes [J]. *Geological Society London Special Publications*, 42: 313–345.
- Wang Xibin, Bao Peisheng, Deng Wanming, Wang Fangguo. 1987. Xizang (Tibet) Ophiolites [M]. Beijing: Geological Publishing House (in Chinese).
- Wu Fuyuan, Liu Chuanzhou, Zhang Liangliang, Zhang Chang, Wang Jiangang, Ji Weiqiang, Liu Xiaochi. 2014. Yarlung Zangbo ophiolite: a critical updated view [J]. *Acta Petrologica Sinica*, 30: 293–325 (in Chinese with English abstract).
- Xiong F, Yang J, Robinson P T, Gao J, Chen Y, Lai S. 2017. Petrology and geochemistry of peridotites and podiform chromitite in the Xigaze ophiolite, Tibet: Implications for a suprasubduction zone origin [J]. *Journal of Asian Earth Science*, 146: 56–75.
- Zhang L L, Liu C Z, Wu F Y, Zhang C, Ji W Q, Wang J G. 2016. Sr–Nd–Hf isotopes of the intrusive rocks in the Cretaceous Xigaze ophiolite, southern Tibet: Constraints on its formation setting [J]. *Lithos*, 258–259: 133–148.
- Zhang Qi, Zhou Guoqin, Wang Yan. 2003. The distribution of time and space of Chinese ophiolites, and their tectonic settings [J]. *Acta Petrologica Sinica*, 19: 1–8 (in Chinese with English abstract).
- Zhang Qi. 2015. Some problems on the Xigaze ophiolite [J]. *Acta Petrologica Sinica*, 31: 37–46 (in Chinese with English abstract).

附中文参考文献

- 陈根文, 刘睿, 夏斌, 邓腾. 2015. 西藏吉定蛇绿岩地球化学特征及其构造指示意义[J]. *岩石学报*, 31: 2495–2507.
- 李文霞, 赵志丹, 朱弟成, 董国臣, 周肃, 莫宣学, DePaolo D J, Dilek Y. 2012. 西藏雅鲁藏布蛇绿岩形成构造环境的地球化学鉴别[J]. *岩石学报*, 28: 1663–1673.
- 牛晓露, 赵志丹, 莫宣学, DePaolo D J, 董国臣, 张双全, 朱弟成, 郭铁鹰. 2006. 西藏日喀则地区德村—昂仁蛇绿岩内基性岩的元素与 Sr–Nd–Pb 同位素地球化学及其揭示的特提斯地幔域特征[J]. *岩石学报*, 22: 2875–2888.
- 潘桂棠, 李兴振, 王立全, 丁俊, 陈智梁. 2002. 青藏高原及邻区大地构造单元初步划分[J]. *地质通报*, 21: 701–707.
- 余宇伟, 朱祥坤, 何源, 马健雄, 孙剑. 2017. 西藏雅鲁藏布构造带日喀则蛇绿岩中新发现豆荚状铬铁矿化[J]. *中国地质*, 44: 610–611.
- 王希斌, 鲍佩声, 邓万明, 王方国. 1987. 西藏蛇绿岩[M]. 北京: 地质出版社.
- 吴福元, 刘传周, 张亮亮, 张畅, 王建刚, 纪伟强, 刘小驰. 2014. 雅鲁藏布蛇绿岩——事实与臆想[J]. *岩石学报*, 30: 293–325.
- 张旗, 周国庆, 王焰. 2003. 中国蛇绿岩的分布、时代及其形成环境[J]. *岩石学报*, 19: 1–8.
- 张旗. 2015. 日喀则蛇绿岩研究中的几个问题[J]. *岩石学报*, 31: 37–46.